Earthquake Engineering & Structural Dynamics
The Journal of the International Association for Earthquake Engineering

EARTHQUAKE ENGINEERING & STRUCTURAL DYNAMICS
Earthquake Engng Struct. Dyn. (2015)
Published online in Wiley Online Library (wileyonlinelibrary.com). DOI: 10.1002/eqe.2568

The effect of seismic uplift on the shell stresses of liquid-storage tanks

Miguel Ormeño*,†, Tam Larkin and Nawawi Chouw

Department of Civil and Environmental Engineering, The University of Auckland, Auckland Mail Centre, Private Bag 92019, Auckland 1142, New Zealand

SUMMARY

Previous theoretical studies have shown that tank uplift, that is, separation of the tank base from the foundation, generally reduces the base shear and the base moment. However, there is a paucity of experimental investigations concerning the effect of uplift on the tank wall stresses, which is the principal parameter that controls the seismic design of liquid-storage tanks. This paper reports a series of shake table experiments on a polyvinyl chloride model tank containing water. A comparison of the seismic behaviour of the tank with and without anchorage is described. Stochastically generated ground motions, based on a Japanese design spectrum, and three tank aspect ratios (liquid-height/radius) are considered. Measurements were made of the stresses at the outer shell of the tank, the tank wall acceleration and the horizontal displacement at the top of the tank. While the top displacement and the tank shell acceleration increased when uplift was allowed, axial compressive stresses decreased by between 35% and 64% with tank uplift. The effect of uplift on the hoop stresses was variable depending on the aspect ratio. A comparison of experimental values with a numerical model is provided. Copyright © 2015 John Wiley & Sons, Ltd.

Received 14 September 2014; Revised 14 January 2015; Accepted 16 January 2015

KEY WORDS: storage tanks; uplift; fluid-structure interaction; scaled model

1. INTRODUCTION

It is important to ensure the post-earthquake functionality of lifelines for the supply of essential resources, such as fuel and water. Much research on the dynamic behaviour of liquid-storage tanks [1–3] has been performed. Based on this, a number of design guides have been developed, discussed and compared [4]. Despite the development of design specifications, field investigations reported in the literature [5–7] have shown that large earthquakes still caused severe damage to storage tanks or even collapse in some cases. This brings a twofold effect: a) economic loss due to tank and pipe damage and b) affected communities are denied access to basic supplies of potable water, water for fire fighting and energy after the seismic event.

Current standards for seismic design are based mainly on the spring-mounted masses analogy proposed by Housner [1]. This analogy is established based on the assumption that liquid-storage tanks behave mainly in two vibration modes. The portion of the liquid contents that moves as if rigidly connected to the tank shell is known as the impulsive mass, m_i (Figure 1). The portion of the contents that moves independently in the tank shell and develops a sloshing motion is called the convective mass, m_c. The predominant mode of vibration of liquid-storage tanks during an earthquake is the impulsive mode [8–10], and its period is very short; generally, a few tenths of a

*Correspondence to: Miguel Ormeño, Department of Civil and Environmental Engineering, The University of Auckland, Auckland Mail Centre, Private Bag 92019, Auckland 1142, New Zealand.
†E-mail: morm010@aucklanduni.ac.nz

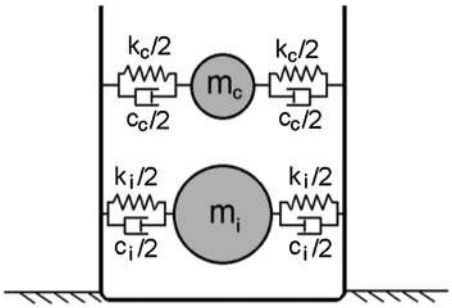

Figure 1. Spring-mounted masses analogy for liquid storage tanks.

second. The convective mode becomes more influential in squat tanks, and the period is considerably longer.

An observable phenomenon that has been little studied in liquid-storage tanks is uplift of the base of the tank. Uplift is the physical separation of the tank base from the tank foundation during seismic motion. The first studies of storage tanks assumed the structure to be fixed to the base. However, this fixity condition does not always occur in the field; in fact, many storage tanks are not provided with anchorage, and thus, these structures can uplift.

The beneficial influence of partial uplift on structures has been identified and reported several decades ago, for example, [11–14]. However, current standards and recommendations for storage tanks (e.g. [15, 16]) provide a conservative seismic design for unanchored tanks [4]. These documents affirm that uplift of structures should be avoided because it has the potential to lead to structural collapse. The very limited amount of investigation carried out into this matter has established the belief that structural uplift will increase collapse potential. This is the source of the impediment of considering the beneficial effect of uplift in seismic design.

In most research studies, the structure was assumed to be rigid [17, 18]. For this reason, only the rocking performance of the rigid body was considered in these investigations, while the natural modes of the structures were ignored. Kodama and Chouw [19] demonstrated the significance of structural flexibility by showing that the uplift behaviour of flexible structures is different from that of rigid structures. Qin *et al.* [20] showed that uplift can reduce plastic hinge development of the structure. Loo *et al.* [21] described the effectiveness of slip-friction connectors as a hold-down mechanism to control the uplift behaviour of flexible structures.

Specifically in the case of liquid-storage tanks, Wozniak and Mitchell [2] included in their work a solution for unanchored tanks allowing uplift, but in their solution, they neglected the membrane effects in the base plate. Ishida and Kobayashi [22], and Malhotra and Veletsos [23] investigated the behaviour of unanchored tanks by using small deflection beam theory to model the bottom plate of the tanks. Both these works give the relationship between bending moment of the beam and uplift (vertical displacement) of the extreme fibre of the tank base at the junction with the tank wall (Figure 2). In their subsequent works, Malhotra and Veletsos [24, 25] provide a relationship between base rotation and base moment leading to an evaluation of the seismic response of storage tanks including uplift for a given ground motion.

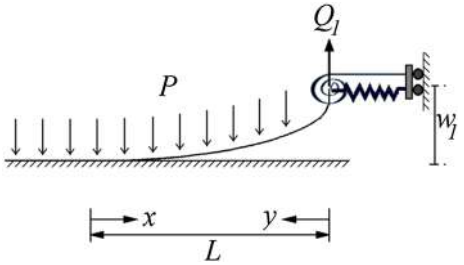

Figure 2. Beam model used in [23] to represent a strip of the bottom plate.

DOI: 10.1002/eqe

P = uniform pressure on the bottom plate
Q_1 = upward force on a strip of the bottom plate resulting from the overturning moment
w_1 = uplift due to the upward force; and
L = uplifted length of the beam in the model

The constraints shown on the right hand side of the beam in Figure 2 correspond to the motion restriction imposed by the tank wall on the bottom plate. Malhotra [26] used the base plate moment–rotation relationship given in [24] (Figure 3) to carry out a simplified nonlinear analysis for performance-based seismic design of tanks. In the example given in [26], the overturning moment and base shear were reduced by more than 70% from that of the equivalent fully anchored tank. This reduction results from uplift occurring in the unanchored tank, and in this way, the bottom plate can deform plastically.

From Figure 3, Malhotra [26] found the force–displacement relationship of the impulsive mass, m_0, and the equivalent viscous damping of the tank with uplift. This enabled the computation of the decrease in the earthquake-induced base shear and overturning moment using a simplified nonlinear analysis for the performance-based seismic design of the tank, which included the determination of the acceleration–deformation spectrum (demand curve).

Ormeño *et al.* [27] carried out experimental work on the effect of uplift on the displacement and acceleration of a tank shell. However, this work does not contain an experimental investigation into the effect of uplift on the tank shell stress, which is the principal parameter controlling the design.

The objective of the work reported here is to quantify the effect of uplift on storage tanks in terms of the axial and hoop stresses of the tank wall. The study entails the use of a polyvinyl chloride (PVC) model tank that is subjected to earthquake motion on a shake table. To the best of the author's knowledge, an experimental investigation on stress development in the tank shell with uplift has never been reported in the literature. Successful development of methods to predict the uplift of storage tanks, based at least in part on experimental data, will open the way to more realistic design techniques.

2. METHODOLOGY

2.1. Tank model

A physical model consisting of a cylindrical PVC tank (Figure 4) was used to represent a prototype steel tank. The Buckingham π theorem [28] was applied to meet the similitude conditions between the scale model and the prototype. In practice, most seismic design of storage tanks can be achieved using a single-degree-of-freedom (SDOF) system based on the impulsive mode of vibration [8]. In

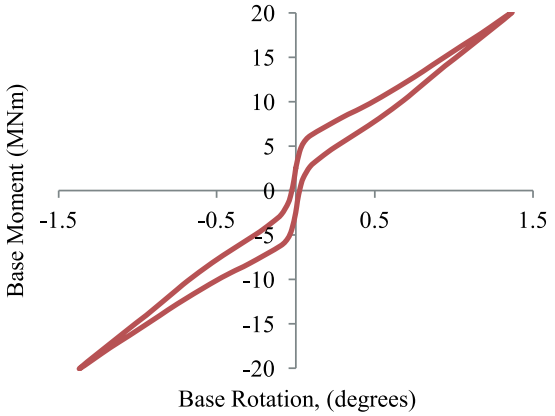

Figure 3. Uplift resistance of the base plate from Malhotra [26].

DOI: 10.1002/eqe

Figure 4. Experimental polyvinyl chloride model on the shake table.

this way, the Cauchy number, as defined by [20], is considered to meet the requirements of similitude. This relation is shown in Equation (1):

$$\frac{F_i}{F_e} = \frac{m \cdot a}{k \cdot u}, \tag{1}$$

where

F_i = inertial force
F_e = elastic restoring force
m = mass of the system m_i (Figure 1)
a = horizontal acceleration
k = translational stiffness k_i (Figure 1); and
u = horizontal deflection.

A good approximation for computing the impulsive mass of the system is to consider only the impulsive mass of the liquid, that is, the mass of the tank wall will not be included in the impulsive mass. In this way, because the model and the prototype store the same liquid (water), the length scale factor determines the mass scale factor. The stiffness (k) is determined by the geometry and the mechanical properties of the tank and liquid. Once these properties are set in the model and prototype, the only variable that can be adjusted to meet the requirement of the relationship of Equation (1) is the acceleration (a). Equation (2) shows the dimension of acceleration.

$$[a] = [l] \cdot [t]^{-2}, \tag{2}$$

where

l = length; and
t = time.

However, length (l) is already set; therefore, the time scale factor must be adjusted to meet the requirement of Equation (1). The dimensions and properties of the model and prototype are shown in Table I. Scale factors for the experiment are shown in Table II.

DOI: 10.1002/eqe

Table I. Dimensions and properties of tank model and prototype.

	Model	Prototype
Material	PVC	Steel
Young's modulus (MPa)	$1.6 * 10^3$	$2.068 * 10^5$
Density of the tank shell material (kg/m^3)	1200	7850
Yield stress (MPa)	25	250
Diameter (m)	0.50	10.00
Height (m)	0.75	15.00
Wall and base thickness (mm)	4	10
Mass of the contents (kg)	147	1178097

The values given correspond to an aspect ratio of 3.

Table II. Scale factors.

Dimension	Scale factor
Length	20
Mass (liquid content only)	8000
Time	4.64
Stiffness	369.5
Acceleration	0.93
Force	7440

The model was not provided with a roof to enable comparison with the theoretical equations given by the current standards and design recommendations for computing the properties and seismic response of storage tanks. These documents assume that the top of the tank wall is not stiffened by ring girders or a roof structure. This approximation is satisfactory for most practical cases where the tank is provided with a roof [16].

Three different liquid levels were considered in order to investigate the sensitivity of the response to different liquid height to radius ratios (aspect ratio). The liquid levels considered were 250 mm, 500 mm and 750 mm to give aspect ratios of 1, 2 and 3.

Two different boundary conditions were invoked in the experimental work: fixed to the shake table and free to uplift. Four bolts were used to anchor the tank to the shake table (Figure 5). Angles of PVC attached to the tank shell were used as anchor bolt brackets. The thickness and size of the angles were selected to ensure they were stiff enough to avoid bending.

A wire transducer was used to measure the top horizontal displacement of the tank (Figure 6). An accelerometer was used to measure the tank wall horizontal acceleration. This instrument was located at a height of 400 mm on the shell of the tank orientated in the direction of the applied motion.

Figure 7(a) shows the location of the strain gauges implemented to measure the axial stresses on the tank shell, while Figure 7(b) shows the radial distribution of the strain gauges to measure the hoop stresses. The strain gauges used to measure the hoop stresses were located at a height of 150 mm.

The equations to compute the dynamic characteristics of the model and prototype were obtained from the New Zealand Society for Earthquake Engineering (NZSEE) recommendations [16]. The period of vibration of the impulsive horizontal mode, T_i, is:

$$T_i = \frac{5.61 \cdot \pi \cdot H}{k_h} \cdot \sqrt{\frac{\gamma_l}{E \cdot g}}, \tag{3}$$

where

H = liquid height
k_h = period coefficient which depends on the ratio of the liquid height to tank radius (Figure 8)
γ_l = unit weight of the liquid

DOI: 10.1002/eqe

Figure 5. Anchor bolt used to fix the tank to the shake table.

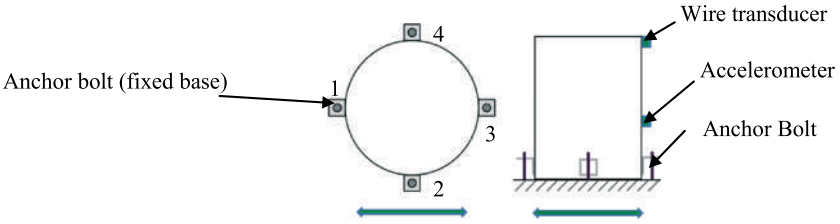

Figure 6. Plan view and elevation of the tank model.

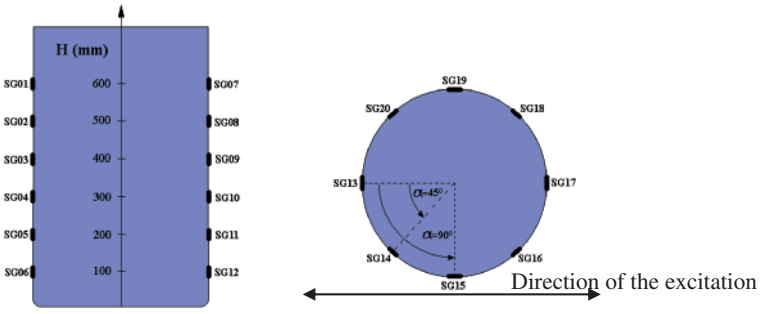

(a) Vertical arrangement of strain gauges in the direction of the excitation

(b) Radial arrangement of strain gauges at 150 mm above the base

Figure 7. Arrangement of the strain gauges at the outer tank surface.

E = Young's modulus of the tank material; and
g = gravitational acceleration.

Using Equation (3) the impulsive period of vibration of the model and prototype for an aspect ratio of 3 is 0.036 s and 0.167 s, respectively.

New Zealand Society for Earthquake Engineering recommendations [16] gives the relationships shown in Figure 9 to determine the modal masses of the tank-fluid system:

DOI: 10.1002/eqe

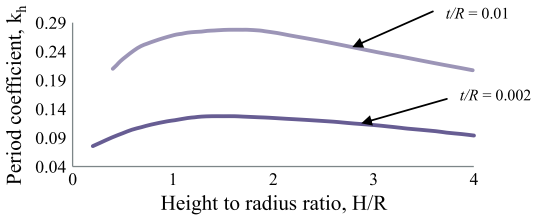

Figure 8. Period coefficient k_h for horizontal tank – liquid mode, from New Zealand Society for Earthquake Engineering recommendations [16].

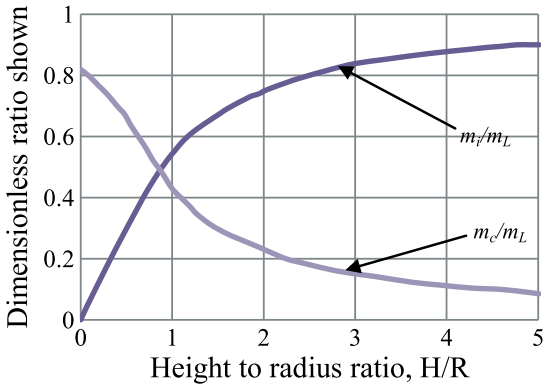

Figure 9. Impulsive and convective mass components, from New Zealand Society for Earthquake Engineering recommendations [16].

where

t = tank wall thickness; and
R = mean radius of the tank.
m_i = impulsive mass
m_c = mass of the first convective mode of vibration
m_L = mass of the fluid.

Once impulsive mass and impulsive period are determined, the impulsive stiffness (k_i) is computed using Equation (4).

$$k_i = \frac{4 \cdot \pi^2 \cdot m_i}{T_i^2} \tag{4}$$

2.2. *Ground motions*

A set of 15 simulated earthquake records were used in testing the tank model. The shake table excitations were numerically simulated ground motions from the Kobe Japanese design spectrum [29] for hard soil conditions [30]. The spectra were constructed by containing the spectral values of the severe ground excitations recorded in the Kobe earthquake within an envelope. The similitude requirement was met by applying the scale factors for acceleration and time shown in Table II. In Figure 10, 3 of these 15 ground motions are plotted.

3. RESULTS

The values shown in the following figures of both stresses, axial compressive and hoop stresses, are the values due to the seismic forces obtained from the model. Shell stresses due to the hydrostatic pressure are not plotted.

DOI: 10.1002/eqe

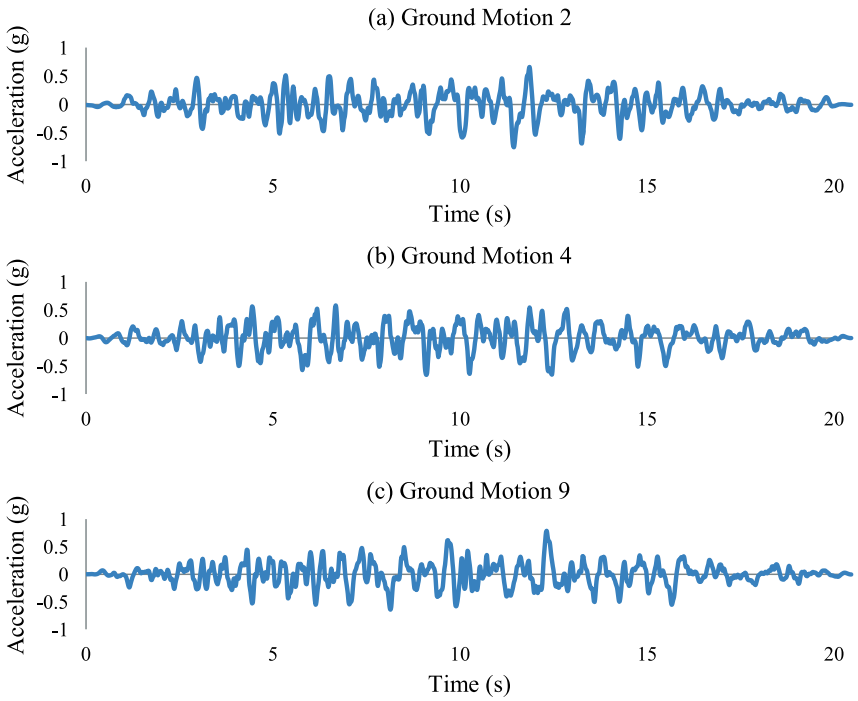

Figure 10. Three of the 15 simulated ground motions used in the study.

3.1. *Axial compressive stresses*

The maximum compressive stresses obtained from three ground motions at the heights shown in Figure 7(a) and for the three aspect ratios considered are shown in Figures 11, 12 and 13.

Figures 11, 12 and 13 show that in the top part of the tank shell for both boundary conditions the maximum axial compressive stress is similar. However, the maximum compression stress is reduced in the locations near the bottom plate when the tank is allowed to uplift. This reduction significantly increases with closer proximity to the base plate. This is a very important finding because the stress at that location is the value that controls the design of cylindrical storage tanks. In most practical cases, the tank shell is not uniform, because the tank shell is formed by several courses of different thickness, with the bottom shell course being the thickest. API 650 [15] does not require a verification of the upper shell courses under seismic conditions if the calculated thickness of the

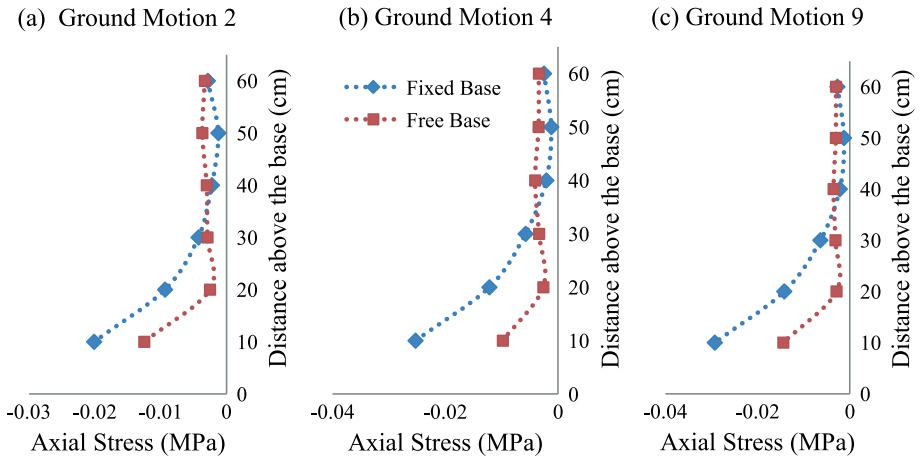

Figure 11. Vertical distribution of shell outer fibre maximum compressive stresses, H/R = 1.

DOI: 10.1002/eqe

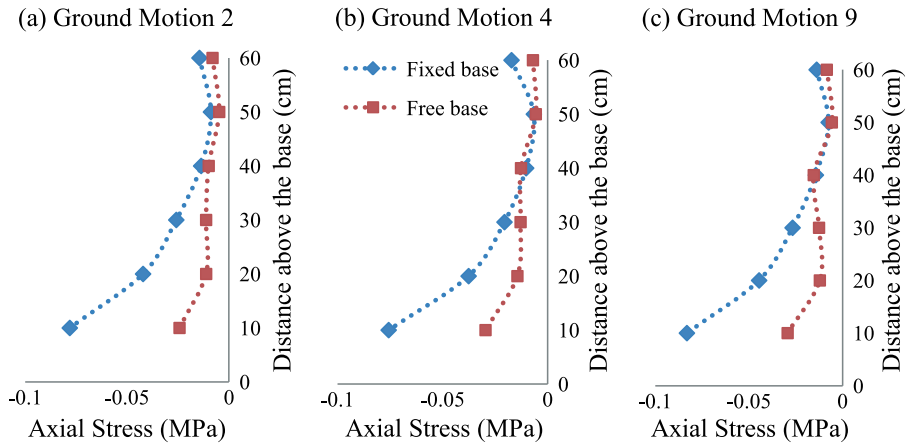

Figure 12. Vertical distribution of shell outer fibre maximum compressive stresses, H/R = 2.

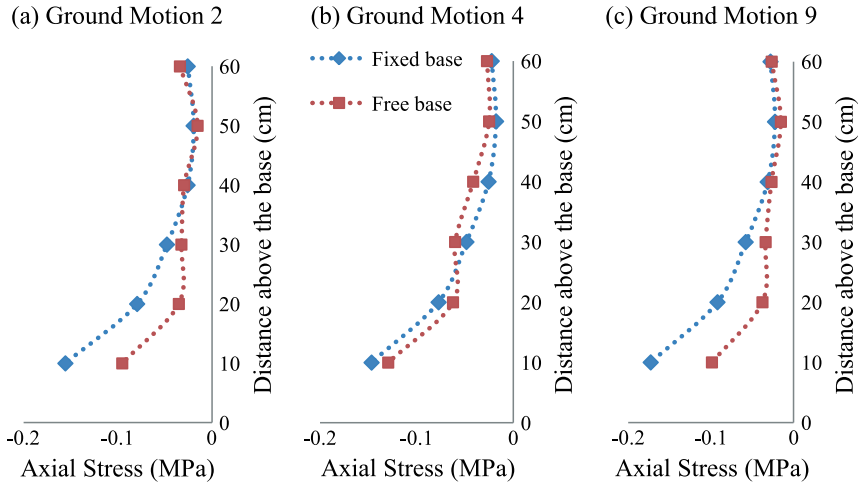

Figure 13. Vertical distribution of shell outer fibre maximum compressive stresses, H/R = 3.

bottom shell course under seismic forces is greater than the thickness required for hydrostatic pressure. In this case, this standard allows an increase in the thickness of the upper shell courses in same proportion as the bottom course. To better understanding how uplift affects the compression stresses at the bottom of the shell (10 cm above the base), the ratio of the maximum compressive stress without anchorage to that with anchorage, MCSR, as defined in Equation (5), is shown in Figure 14 for the 15 ground motions considered. The average value for each aspect ratio is given in brackets.

$$MCSR = \frac{Maximum\ compressive\ stress\ measured\ on\ the\ unanchored\ tank}{Maximum\ compressive\ stress\ measured\ on\ the\ anchored\ tank} \tag{5}$$

Figure 14 shows that, for all earthquake records and aspect ratios, uplift produced lower outer-fibre maximum compressive stresses in the shell 100 mm above the base. This reduction was most significant for an aspect ratio of 2 and least significant for an aspect ratio of 3. A summary of the results, using all earthquake records, is shown in Table III.

A ratio can also be obtained for the maximum top displacement and the maximum tank wall acceleration. Similarly, the MAR may be defined as the ratio of the maximum tank wall horizontal acceleration without anchorage to that with anchorage (Equation (6)), and MDR may be defined as the ratio of the maximum top displacement without anchorage to that with anchorage (Equation (7)).

DOI: 10.1002/eqe

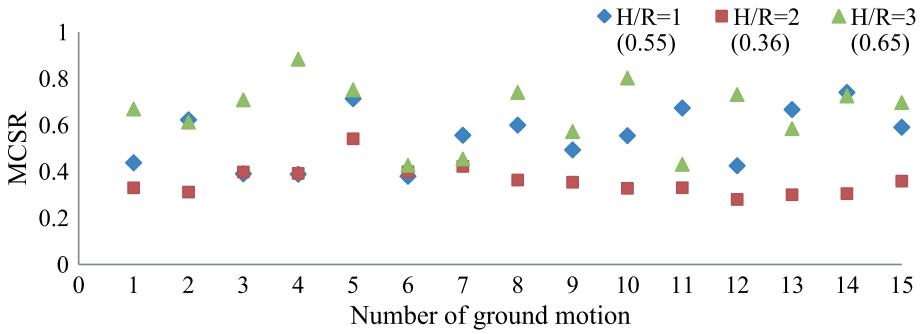

Figure 14. MCSR for the 3 aspect ratios utilised.

Table III. Decrease of the maximum axial compressive stress due to uplift.

H/R	Minimum (%)	Maximum (%)	Average (%)
1	26	62	45
2	46	72	64
3	12	57	35

These two variables are plotted in Figure 15 for the 15 ground motions and the three aspect ratios considered. The average value for each aspect ratio is given in brackets.

$$MAR = \frac{Maximum\ tank\ wall\ acceleration\ measured\ on\ the\ unanchored\ tank}{Maximum\ tank\ wall\ acceleration\ measured\ on\ the\ anchored\ tank} \tag{6}$$

$$MDR = \frac{Maximum\ top\ displacement\ measured\ on\ the\ unanchored\ tank}{Maximum\ top\ displacement\ measured\ on\ the\ anchored\ tank} \tag{7}$$

Whereas the MCSR decreased in all the cases analysed, MAR and MDR increased in approximately 76% and 56% of the cases, respectively. This apparently contradictory result can be explained by

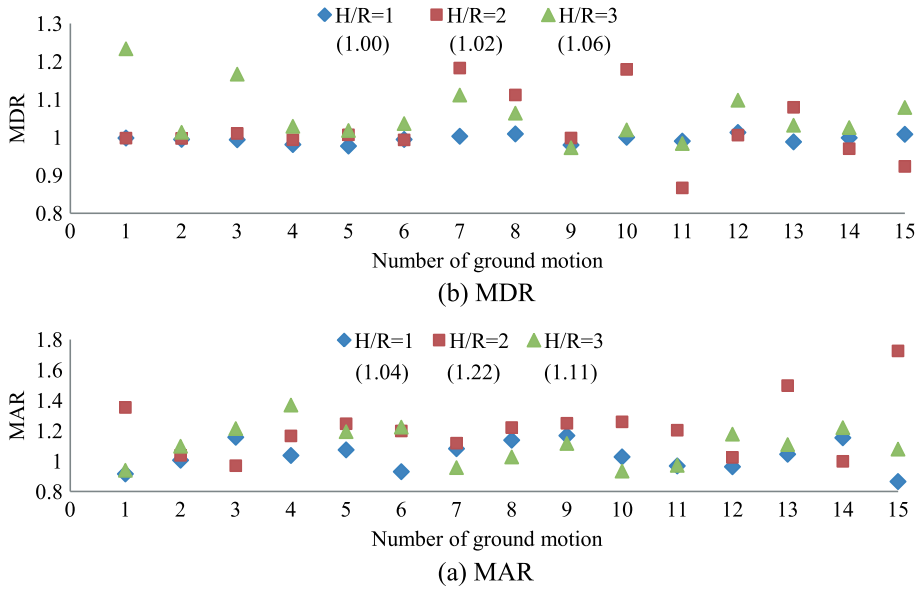

Figure 15. MAR and MDR for the 3 aspect ratios utilised.

DOI: 10.1002/eqe

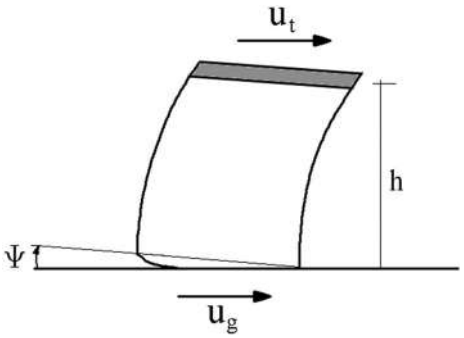

Figure 16. Sketch of an uplifting tank.

considering the situation shown in Figure 16, assuming that the tank can be represented as a SDOF system [8, 10]:

where

u_t = total displacement of the equivalent SDOF system; and
u_g = ground displacement.

Equation (8) defines the total displacement of the SDOF system:

$$u_t = u_g + \Psi \cdot h + u, \tag{8}$$

where

Ψ = base rotation due to uplift
h = height of the equivalent SDOF system; and
u = displacement of the SDOF due to the tank shell deformation.

In Equation (8), the second term on the right hand side (RHS) implies a rigid body rotation of the shell; thus, the first two terms on the right side have no impact on the stresses in the wall of the tank. Only the displacement due to the tank shell deformation (u) is instrumental in producing wall stress through structural distortion. Thus, it is possible to obtain higher horizontal accelerations and displacements when the tank is allowed to uplift but with lower tank wall axial stresses. The shell axial stress is the principal variable that controls tank design. This experimental work establishes that uplift is beneficial because it produces lower axial stresses in the shell. This result is contradicted in current standards and design guides leading to a conservative design for unanchored tanks.

3.2. Hoop stresses

The maximum shell-hoop stresses obtained from three ground motions and for the three aspect ratios and two boundary conditions are shown in Figures 17, 18 and 19. Because of the symmetrical radial arrangement of the strain gauges (Figure 7(b)), the results are shown in the locations that form an angle of 0°, 45° and 90° (SG13, SG14 and SG15) with the load direction.

In most cases, the maximum measured hoop stress was in SG13 ($\alpha = 0°$). At this location, this stress varied more significantly than the other points when the boundary condition was changed. On the other hand, the lowest measured hoop stress was for $\alpha = 90°$ (SG15) in most cases. This point shows the lowest variation also when the fixity condition was modified. From Figures 17, 18 and 19, it is not possible to identify a pattern that explains how uplift affects the hoop stresses of the tank shell's outer fibre. It is possible to identify what locations have the highest variations in hoop stress for the two boundary conditions. However, all these values were obtained at the same height (150 mm). Thus, these current experiments provide no information about hoop stress variation with height; particularly, in the case of variable wall thickness. The important value for design of the shell course is the maximum hoop stress that occurs at the base plate-shell connection. However, the hoop stress was not measured at this location. MHSR, at a distance of 150 mm above the base, may be defined,

DOI: 10.1002/eqe

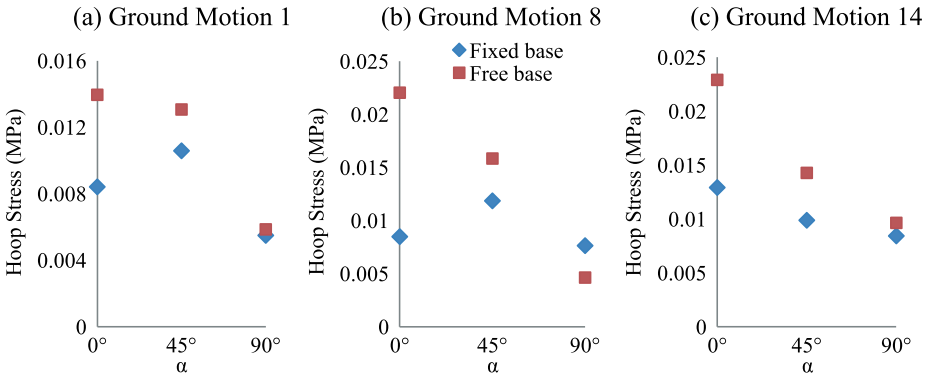

Figure 17. Maximum hoop stresses at the outer tank shell 150 mm above the base, H/R = 1.

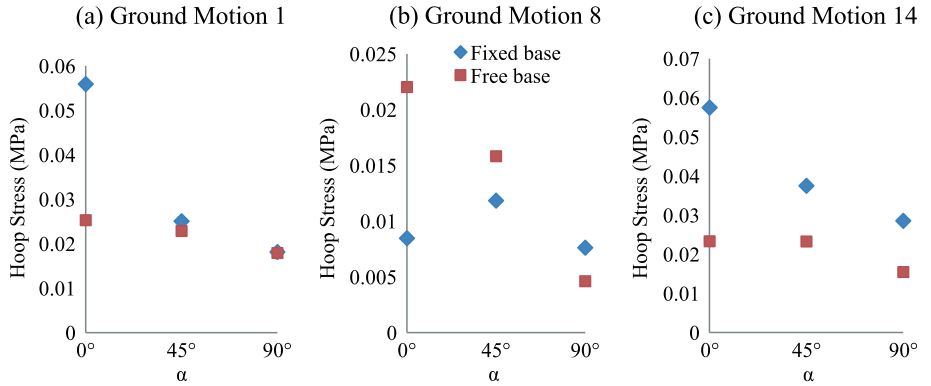

Figure 18. Maximum hoop stresses at the outer tank shell 150 mm above the base, H/R = 2.

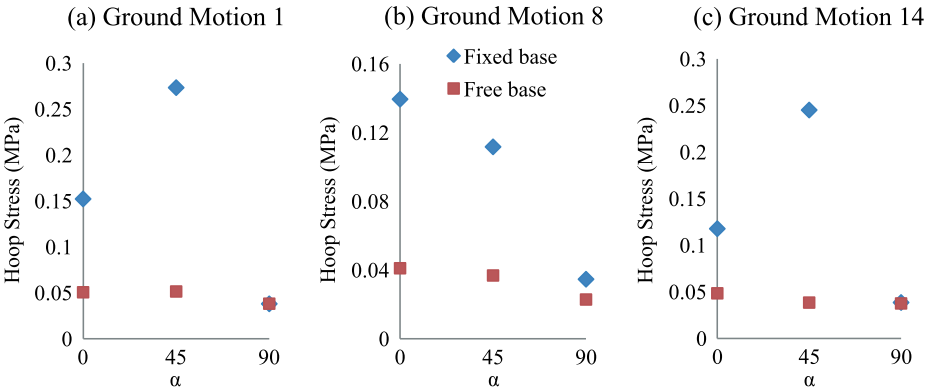

Figure 19. Maximum hoop stresses at the outer tank shell 150 mm above the base, H/R = 3

in a similar way to the analysis for axial stresses, as the ratio of the maximum hoop stress without anchorage to that with anchorage, as given in Equation (9). This ratio is shown in Figure 20 for the 15 ground motions considered. The average value for each aspect ratio is given in brackets.

$$MHSR = \frac{Maximum\ \ hoop\ \ stress\ \ measured\ \ on\ \ the\ \ unanchored\ \ tank}{Maximum\ \ hoop\ \ stress\ \ measured\ \ on\ \ the\ \ anchored\ \ tank} \tag{9}$$

Figure 20 shows that uplift has a different effect on the measured hoop stresses depending on the aspect ratio of the tank considered. For aspect ratios of 2 and 3, where the impulsive mode of

DOI: 10.1002/eqe

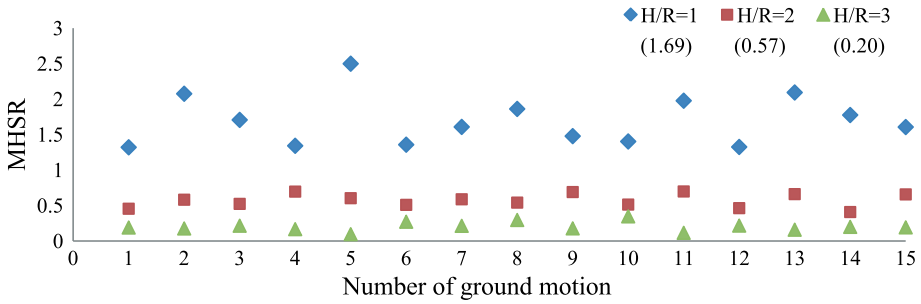

Figure 20. MHSR for the 3 aspect ratios utilised.

vibration is much more influential in the seismic response than the convective mode, uplift is beneficial. On the other hand, when the convective mode becomes comparable in importance to the impulsive mode (H/R = 1), allowing uplift results in higher measured hoop stresses in the tank shell. Current standards and design guides increase the seismic forces [15] or decrease the capacity of the tank shell [16] under conditions of uplift. Thus, in current design practice, uplift is always considered a hazard. However, in the case of slender tanks, this experimental research shows the opposite conclusion for the axial stresses and hoop stresses. In the case of squat tanks, uplift does not reduce the hoop stresses in the tank shell. On the basis of the experiments reported here, squat tanks (H/R = 1) are likely to have higher hoop stresses with uplift present.

The conclusions made in the previous paragraph cannot justifiably be extended to the base plate-shell connection because no measurement was made at that location. A summary of the decrease, using all earthquake records, of the maximum-measured hoop stresses is shown in Table IV.

3.3. Comparison with a numerical model

Numerical studies have been carried out to model the seismic behaviour of storage tanks including uplift. Figure 21 shows the ratio between the results obtained from the numerical model given by Malhotra and Veletsos [24, 25], and Malhotra [31] and the axial stresses obtained in this

Table IV. Decrease due to uplift of the maximum hoop stress.

H/R	Minimum (%)	Maximum (%)	Average (%)
1	−150	−32	−69
2	30	59	43
3	65	91	80

Negative values mean increase.

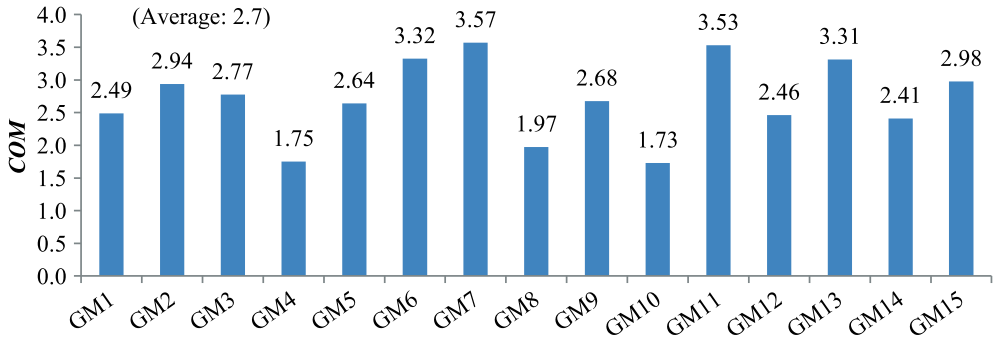

Figure 21. Difference between numerically and experimentally obtained stresses for H/R = 3.

DOI: 10.1002/eqe

experimental study. Equation (10) provided in [31] is used to compute the axial stresses of the numerical model:

$$\sigma_{\text{axial}} = \frac{Q_1}{b \cdot h_s} \tag{10}$$

where

σ_{axial} = axial stress in the tank shell
Q_1 = uplift force acting at the junction of the tank wall and a strip representing part of the base plate computed using the bending solution given by [23] (Figure 2)
b = width of the beam elements (strip) used by [24] to model the base plate; and
h_s = wall thickness.

Figure 21 shows that, for the 15 ground motions, the values given by numerical models are higher than the values obtained from the experiments. On average, the values obtained by the application of the numerical model are 2.7 times higher than those obtained from the shake table tests.

where:

$$COM = \frac{\text{Axial stresses obtained by numerical analysis}}{\text{Axial stresses obtained in the experiments}}$$

Although the experimental values were not obtained precisely from the junction between the wall and the base plate, the differences are still considerable. The main factor that explains this big difference is that the numerical model is based on a stiffer bottom plate than what actually exists. According to the numerical model [24], just one beam is supporting all the compression of the tank wall. For simplicity, Malhotra and Veletsos [24] consider a flexible bottom plate, but to compute the vertical displacement of any strip use only the rotation of the strip with the maximum uplift and an assumed distribution of wall displacement with circumferential distance, that is, the model considers a rigid tank wall. In this way, the circumferential edge of all the beams will lift except one, that is, the beam that is entirely in contact with the foundation. The vertical force Q_1 is the result of the compressive stresses along the bottom edge of this strip. This description of conditions on the bottom plate, using a finite number of strips, consequently leads to a concentration of stress that does not accurately reflect the experimental distribution of stress along the rim. Peek [32] mentions that the case of a single point of the shell in contact with the base is the most basic simplification of the general case. This leads to a higher moment–rotational stiffness of the model bottom plate compared with the physical reality. Consequently, for a given vertical displacement, the vertical force Q_1 calculated at the wall–base junction for any beam using the numerical model is higher than the force actually required. Equation (10) shows that a higher value of Q_1 results in a higher value of the axial stress. In [24], an assumption of a point contact between the wall of steel tank and the base does not represent the condition of the PVC tank considered in this experimental work. Because PVC is softer than steel, a circumferential wall–base contact may occur that resulted in a reduction of the axial stress. This is a similar effect to that caused by a flexible base as reported by Malhotra [31], who found that contact pressure reduces as the support becomes more flexible.

The effects of the factor described earlier can be clearly observed in Figure 22. As what was explained before, the static relationship given by [23, 24] is used to compute uplift and axial stresses for a given earthquake in [25]. Figure 22 shows a comparison of this static relationship using the equations given in [23] and three push-over tests carried out on the PVC model.

The static relationship obtained from the numerical model is on average 2.86 times higher than the average of the three tests carried out. Using the average of the three push-over tests, a relationship between the base rotation and overturning moment can be computed. This relationship is plotted in Figure 23.

DOI: 10.1002/eqe

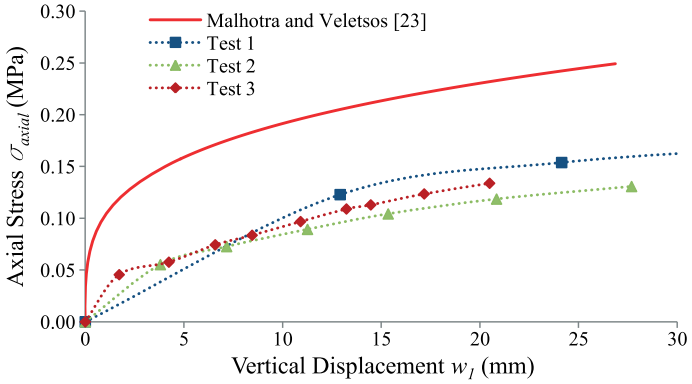

Figure 22. Comparison of axial stress – vertical displacement relationship.

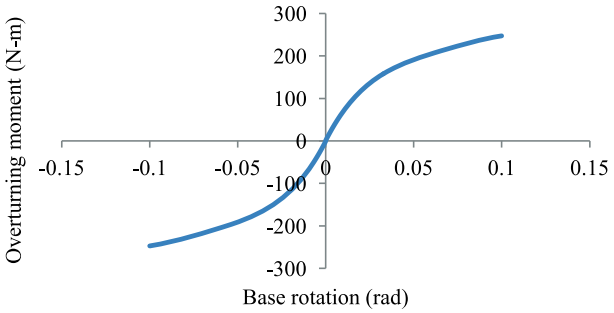

Figure 23. Relationship between overturning moment and base rotation.

It is worth mentioning that Figure 23 does not show evidence of hysteresis from plastic deformation, as shown in Figure 3; rather, it is a nonlinear elastic load-deformation path. For the levels of base rotation of the PVC tank reached in the tests, the elastic limit of the material (PVC) was not exceeded.

As was mentioned earlier, the strain gauge used to calculate the axial stresses on the tank wall is not located at the junction of the base plate and the tank wall. For this reason, an adjustment of the numerical values of axial stresses is required to make the numerical and experimental results directly comparable. Axial stresses are proportional to the moment acting on the cross section of the tank [2, 3]. Hence, because the cross section of the tank is uniform along the height, the ratio between the axial stresses at the bottom and the axial stresses at the height of the strain gauge are the same as the ratio of the moment acting at those heights. Housner [1] defines the impulsive pressure exerted against the tank wall and the resultant force as follows:

$$p_w = -\rho\, a_i H \left(y/H - {}^{1}\!/_{2(y/H)^2}\right)\cdot\sqrt{3}\cdot\cos\varphi\cdot\tanh\left(\sqrt{3}R/H\right) \tag{11}$$

$$P = \int_0^H \int_0^{2\pi} p_w \cos\varphi\, R\, d\varphi\, dy = -\rho\, a_i \pi R^2 H \frac{\tanh\left(\sqrt{3}R/H\right)}{\sqrt{3}R/H} \tag{12}$$

where:

p_w = impulsive pressure exerted against the tank wall
ρ = density of the fluid
a_i = impulsive acceleration of the fluid
H = liquid height
Y = vertical axis (see Figure 24)
ϕ = angle with respect to axis x (Figure 24); and
R = tank radius.

DOI: 10.1002/eqe

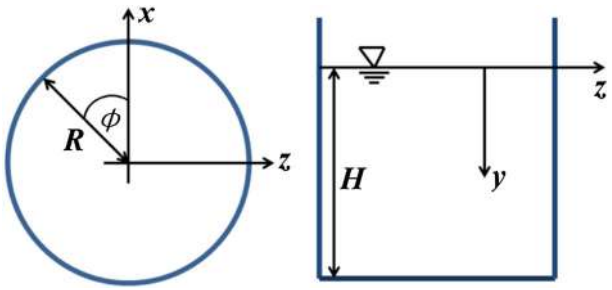

Figure 24. Plan view (left) and elevation of the tank [1].

Equation (11) gives the total horizontal force exerted by fluid on the tank wall, and the point of application of this force is located at 3/8 H above the base [1]. If Equation (11) is solved for $y = H_1$, then the applied horizontal force is the following:

$$P_{y=H_1} = \int_0^{H_1} \int_0^{2\pi} p_w \cos\varphi \, R \, d\varphi \, dy = -\rho \, a_i \, \pi R^2 H_1 \frac{\tanh\left(\sqrt{3}R/H\right)}{\sqrt{3}R/H} \tag{13}$$

and the point of application is located at 3/8 H_1 above $y = H_1$. Because the moment acting on the cross section is equal to the product of the resultant force and the distance of this force from the cross section analysed, the ratio of the moment acting on $y = H_1$ and the one acting on the tank base is as follows:

$$\frac{M_{y=H_1}}{M_{bottom}} = \frac{{H_1}^2}{H^2} \tag{14}$$

In the experiments, $H = 0.75$ m (liquid level) and $H_1 = 0.65$ m (location of the strain gauge); therefore, the axial stresses calculated by the numerical analysis must be multiplied by 0.75 to directly compare the numerical values with those obtained from the experiments. Applying this correction and using the relationship shown in Figure 23, the ratio between the axial stresses obtained from the experiment, and those calculated using the numerical model have been re-computed and are given in Figure 25:

where

$$COM2 = \frac{\text{Axial stresses obtained by numerical analysis using the empirical stiffness}}{\text{Axial stresses obtained in the experiments}}$$

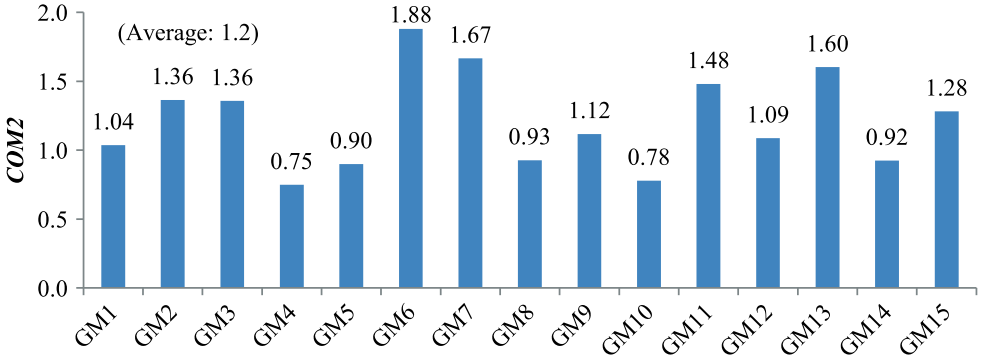

Figure 25. Comparison of axial stresses using the updated static stiffness and height of gauge adjustment, for H/R = 3.

DOI: 10.1002/eqe

Figure 25 shows a closer match of the axial stresses than those shown in Figure 21. It is clear that the assumptions behind the numerical model overestimate the axial stresses in the tank wall because of a stiffer base plate and a rigid tank wall compared with the experimental values determined from the physical model. For these reasons, the numerical approach described, [24, 25], to calculate seismically induced shell stresses of liquid-storage tanks with uplift needs to be reconsidered.

4. CONCLUSIONS

A series of experiments on a model PVC liquid-storage tank, with three aspect ratios, have been considered. The main aim was to determine the effect of base plate uplift on the outer surface shell stresses of tanks using 15 scaled simulated earthquake motions.

The investigations revealed the following:

(1) Uplift lowers the axial compressive stresses on the tank shell. For all ground motions and aspect ratios when uplift took place, the maximum average compressive stress decreased from 35% to 64%. Because PVC is softer than steel, these results cannot be justifiably generalised for steel tanks. Furthermore, the measurements were not made at the point of maximum axial stress.
(2) In most of the experiments, using anchored and unanchored tanks, the highest hoop stresses were obtained at the point that lays on the central vertical plane of the tank shell, that is, the vertical plane in the line of action of the acceleration applied. Generally, the lowest values of hoop stress were obtained at the point that has maximum eccentricity with respect to the central vertical plane of the tank.
(3) The effect of uplift on the maximum measured hoop stress was found to be a function of aspect ratio. For aspect ratios of 2 and 3, uplift reduced the maximum value compared with that of the anchored case. For an aspect ratio of 1, uplift increased the maximum hoop stress. Squat tanks under uplift may experience higher hoop stresses compared with the anchored case.
(4) With uplift, the maximum tank acceleration increased in 76% of the experiments. Similarly, in 56% of cases, the maximum top displacement was higher under uplift.
(5) The numerical model of unanchored tanks considered here overestimates the value of axial stress because of the assumptions made in the theory of the model.

ACKNOWLEDGEMENTS

The authors wish to thank the Chilean Government for awarding the first author with the scholarship ‘Becas Chile’ for his doctoral study at the University of Auckland and the Ministry of Business, Innovation and Employment through the National Hazards Research Platform, award number UoA3703249, for the support of this research. The authors would like to thank Professor A. Chopra for his helpful correspondence that considerably enhanced the content of the manuscript and the reviewer for the constructive comments.

REFERENCES

1. Housner GW. Dynamic pressures on accelerated fluid containers. *Bulletin of the Seismological Society of America* 1957; **47**:15–35.
2. Wozniak RS, Mitchell WW. Basis of seismic design provisions for welded steel oil storage tanks. *API Refining 43rd* 1978.
3. Veletsos AS. Seismic response and design of liquid storage tanks. Guidelines for the seismic design of oil and gas pipeline systems. *Technical Council on Lifeline Earthquake Engineering (ASCE) New York* 1984; 255–370.
4. Ormeño M, Larkin T, Chouw N. Comparison between standards for seismic design of liquid storage tanks with respect to soil–foundation–structure interaction and uplift. *Bulletin of the New Zealand Society for Earthquake Engineering* 2012; **45**:40–46.
5. Haroun MA. Behavior of unanchored oil storage tanks: Imperial Valley earthquake. *Journal of Technical Topics in Civil Engineering (ASCE)* 1983; **109**(1):23–40.
6. Manos GC, Clough RW. Tank damage during the May 1983 Coalinga earthquake. *Earthquake Engineering and Structural Dynamics* 1985; **13**(4):449–466.
7. Cooper TW. A study of the performance of petroleum storage tanks during earthquakes, 1933–1995. *NIST No. GCR 97-720*, *U.S. Dept. of Commerce*, *National Institute of Standards and Technology*, *Gaithersburgh*, *Md.* 1997.
8. Larkin T. Seismic response of liquid storage tanks incorporating soil–structure interaction. *Journal of Geotechnical and Geoenvironmental Engineering, ASCE* 2008; **134**(12):1804–1814.

DOI: 10.1002/eqe

9. Veletsos AS, Tang Y, Tang HT. Dynamic response of flexibly supported liquid-storage tanks. *Journal of Structural Engineering, ASCE* 1992; **118**(1):264–283.
10. Malhotra PK. Seismic response of soil-supported unanchored liquid-storage tanks. *Journal of Structural Engineering, ASCE* 1997; **123**(4):440–450.
11. Housner GW. The behavior of inverted pendulum structures during earthquakes. *Bulletin of the Seismological Society of America* 1963; **53**:403–417.
12. Meek JW. Effects of foundation tipping on dynamic response. *Journal of Structural Division (ASCE)* 1975; **101**(7):1297–1311.
13. Huckelbridge AA, Clough RW. Seismic response of an uplifting building frame. *Journal of Structural Division (ASCE)* 1977; **104**(8):1211–1229.
14. Psycharis IN. Dynamics of flexible systems with partial lift-off. *Earthquake Engineering and Structural Dynamics* 1983; **11**:501–521.
15. Welded steel tanks for oil storage. API Standard 650, 11th Edition. *American Petroleum Institute* (*API*) 2007.
16. Seismic design of storage tanks. Recommendations of a study group of the New Zealand National Society for Earthquake Engineering. (*NZSEE*) 2009.
17. Apostolou M, Gazetas G, Garini E. Seismic response of slender rigid structures with foundation uplifting. *Soil Dynamics and Earthquake Engineering* 2007; **27**:642–654.
18. Taniguchi T. Non-linear response analyses of rectangular rigid bodies subjected to horizontal and vertical ground motion. *Earthquake Engineering and Structural Dynamics* 2002; **31**:1481–1500.
19. Kodama T, Chouw N. Soil-structure interaction with uplift due to near-source earthquakes. *Proceedings of the 5th European Conference on Structural Dynamics*, *September 2-5*, *T. U. München*, *Germany* 2002; 1375–1380.
20. Qin X, Chen Y, Chouw N. Effect of uplift and soil nonlinearity on plastic hinge development and induced vibrations in structures. *Advances in Structural Engineering* 2013; **16**(1):135–147.
21. Loo W, Quenneville P, Chouw N. A numerical study of the seismic behavior of timber shear walls with slip-friction connectors. *Engineering Structures* 2012; **34**:233–243.
22. Ishida K, Kobayashi N. An effective method of analyzing rocking motion unanchored cylindrical tanks including uplift. *Journal of Pressure Vessel Technology (ASME)* 1988; **110**:76–87.
23. Malhotra PK, Veletsos AS. Beam model for base uplifting analysis of cylindrical tanks. *Journal of Structural Engineering, ASCE* 1994; **120**(12):3471–3488.
24. Malhotra PK, Veletsos AS. Uplifting analysis of base plates in cylindrical tanks. *Journal of Structural Engineering, ASCE* 1994; **120**(12):3489–3505.
25. Malhotra PK, Veletsos AS. Uplifting response of unanchored liquid-storage tanks. *Journal of Structural Engineering, ASCE* 1994; **120**(12):3525–3547.
26. Malhotra PK. Practical nonlinear seismic analysis of tanks. *Earthquake Spectra* 2000; **16**(2):473–492.
27. Ormeño M, Larkin T, Chouw N. Influence of uplift on liquid storage tanks during earthquakes. *Coupled Systems Mechanics* 2012; **1**(4):311–324.
28. Buckingham E. Illustrations of the use of dimensional analysis on physically similar systems. *Physics Review* 1914; **4**(4):354–377.
29. Chouw N, Hao H. Study of SSI and non-uniform ground motion effect on pounding between bridge girders. *Soil Dynamics and Earthquake Engineering* 2005; **25**:717–728.
30. Earthquake resistant design codes in Japan. *Japan Society of Civil Engineers (JSCE)*. Maruzen: Tokyo, 2000.
31. Malhotra P. Base uplifting analysis of flexibly supported liquid-storage tanks. *Earthquake Engineering and Structural Dynamics* 1995; **24**:1591–1607.
32. Peek R. Analysis of unanchored liquid storage tanks under seismic loads. *California Institute of Technology* 1986.

DOI: 10.1002/eqe